Cryogenics 63 (2014) 94–101

Contents lists available at ScienceDirect

Cryogenics

journal homepage: www.elsevier.com/locate/cryogenics

Performance optimization of a miniature Joule–Thomson cryocooler using numerical model

P.M. Ardhapurkar [a,b], M.D. Atrey [a,*]

[a] Mechanical Engineering Department, IIT Bombay, Mumbai 400 076, India
[b] S.S.G.M. College of Engineering, Shegaon 444 203, India

ARTICLE INFO

Article history:
Received 14 April 2014
Received in revised form 9 July 2014
Accepted 15 July 2014
Available online 27 July 2014

Keywords:
Joule–Thomson cryocooler
Heat exchanger
Optimization
Cooling capacity
Performance

ABSTRACT

The performance of a miniature Joule–Thomson cryocooler depends on the effectiveness of the heat exchanger. The heat exchanger used in such cryocooler is Hampson-type recuperative heat exchanger. The design of the efficient heat exchanger is crucial for the optimum performance of the cryocooler.

In the present work, the heat exchanger is numerically simulated for the steady state conditions and the results are validated against the experimental data available from the literature. The area correction factor is identified for the calculation of effective heat transfer area which takes into account the effect of helical geometry. In order to get an optimum performance of the cryocoolers, operating parameters like mass flow rate, pressure and design parameters like heat exchanger length, helical diameter of coil, fin dimensions, fin density have to be identified. The present work systematically addresses this aspect of design for miniature J–T cryocooler.

1. Introduction

Joule–Thomson (J–T) cryocoolers have been widely used for many applications such as cooling of infrared detectors, cryosurgery probes, thermal cameras, and missile guidance systems, due to their special features such as simple configuration, compact structure and rapid cooldown characteristics. It consists of a recuperative heat exchanger, an expansion device, and an evaporator. Fig. 1 shows the schematic of a J–T cryocooler. The thermodynamic performance of these cryocoolers is mainly governed by the effectiveness of the heat exchanger. Usually, the heat exchanger is Hampson-type finned tube heat exchanger. The finned tubes are helically wound on mandrel and shield is provided on the outside of the coil. The working fluid such as nitrogen, argon at high pressure flows inside the helically coiled finned tube, and returns over the fins after expansion through an orifice at the end of heat exchanger. The low-pressure stream circulates over the finned tube surface in opposite direction to the high-pressure stream. The process 1–2 represents the heat rejection by the hot fluid at high pressure, whereas the process 4–5 is the heat gain by the cold fluid at low pressure.

Several researchers have worked to compute steady state performance of the J–T cryocooler [1–4]. Few studies on transient analysis of J–T cryocooler have also been reported in the literature [5–7]. The design of Hampson-type heat exchanger is crucial due to its complex geometry, variation in thermo-physical properties of fluid and thermal losses. Ng et al. [1] and Xue et al. [2] reported experimental and numerical study of the J–T cryocooler for steady-state characteristics with argon as a working fluid. Chua et al. [4] have argued that, Ng et al. [1] and Xue et al. [2], in their numerical work, have not used the actual heat transfer area for the low pressure return stream in the helical heat exchanger, but have used some correction factors to compute effective area of heat transfer in the return line. Additionally, there is very little information available in the literature related to the effect of various operating and design parameters on the performance of the J–T cryocooler.

The design of recuperative heat exchanger for its optimum performance depends on many parameters such as type of fluid, mass flow rate, supply pressure, and various design parameters such as heat exchanger length, fin tube diameter, helical diameter of coil, fin dimensions, and fin density. In the present work, numerical simulation of the heat exchanger is performed to carry out the parametric study for the optimum performance of the cryocooler.

2. Numerical model of heat exchanger

2.1. Heat exchanger geometry

2.1.1. Calculation of flow area for low pressure stream in shell side

In the present study, the specifications of the heat exchanger are taken from the literature [1], which are given in Table 1. The

* Corresponding author. Tel.: +91 22 2576 7522; fax: +91 22 2572 6875.
E-mail addresses: pm_ardhapurkar@yahoo.com (P.M. Ardhapurkar), matrey@iitb.ac.in (M.D. Atrey).

http://dx.doi.org/10.1016/j.cryogenics.2014.07.006
0011-2275/

Nomenclature

A	area, m^2
A_s	surface area, m^2
Cp	specific heat capacity, J/kg K
d	diameter, m
d_f	fin tube diameter, m
D_h	hydraulic diameter, m
D_{hel}	mean diameter of helical coil, m
f	friction factor
G	mass flux, kg/m^2 s
h	heat transfer coefficient, w/m^2 K
k	thermal conductivity, w/m K
L	length of heat exchanger, m
$\dot{m}$	mass flow rate, kg/s
n	fin density, number of fins per meter
$N_{fins/coil}$	number of fins per coil turn
P	pressure, Pa
p	perimeter of heat transfer, m
Pr	Prandtl number
Re	Reynolds number
t	mean fin thickness, m
T	temperature, K
u	mean velocity, m/s

Greek symbol

ΔP	pressure drop, Pa
ρ	density, kg/m^3

Subscripts

a	ambient
c	cold fluid
ci	capillary inside
co	capillary outside
h	hot fluid
i	inside
in	inlet
m	mandrel
mi	mandrel inside
mo	mandrel outside
o	outside
out	outlet
r	radiation
s	shield
si	shield inside
so	shield outside
w	wall

accurate calculation of the flow area for the low-pressure stream is essential for modeling the finned tube heat exchanger. Fig. 2 shows the cross-section of the finned tube heat exchanger. In order to calculate flow area for low pressure stream, A_c, cross-sectional area of tube without fins and area of fins in one coil turn is subtracted from the total annular area between shield and mandrel. It is expressed in Eq. (1)

$$A_c = \frac{\pi}{4}(d_{si}^2 - d_{mo}^2) - \frac{\pi}{4}[(D_{hel} + d_{co})^2 - (D_{hel} - d_{co})^2] - t(d_f - d_{co}) \times N_{fins\ per\ coil} \quad (1)$$

where d_{si} is inside diameter of shield, d_{mo} is outside diameter of mandrel, D_{hel} is diameter of the helical coil, d_f is finned tube diameter, d_{co} is the fin root diameter, and t is mean thickness of the fin. $N_{fins\ per\ coil}$ represents the number of fins per turn of the coil, which is given in Eq. (2).

$$N_{fins\ per\ coil} = \frac{\pi D_{hel}}{\text{fin pitch}} \quad (2)$$

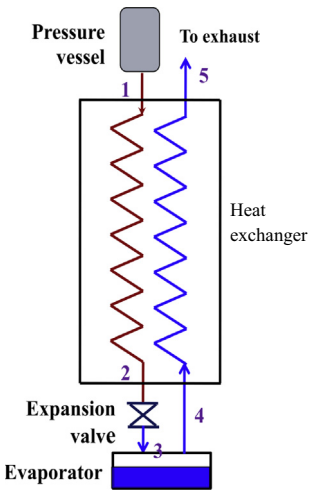

Fig. 1. J–T cryocooler.

Alternatively, the projected area method [8] can be used to calculate flow area and outside perimeter of the finned tube. According to this method, the total available free flow area on shell side, A_c, neglecting diametrical clearance is given in Eq. (3).

$$A_c = \pi D_{hel}[(d_f - d_{co})(1 - n \times t)] \quad (3)$$

where n is number of fins per m.

2.1.2. Calculations of surface area & Perimeter of finned tube

In order to calculate outside perimeter of the finned tube, calculations are done for one turn of the coil neglecting the surface area of tips of the fins. The outside surface area of finned tube is calculated by subtracting surface area occupied by base of all fins on tube in one coil turn from the surface area of bare capillary tube and the surface area of two sides of all fins in one coil turn. Therefore, surface area offered by the outer finned surface in one coil turn, A_s, is calculated as given in Eq. (4).

$$A_s = \pi^2 \left[\frac{n}{2}(d_f^2 - d_{co}^2) + d_{co}(1 - nt)\right] D_{hel} \quad (4)$$

Hence, perimeter of outer finned surface (surface area per unit axial length), p_{co}, is obtained as

Table 1
Specifications of the heat exchanger [1].

Parameters	Dimension
Inside diameter tube, d_{ci} (mm)	0.3
Outside diameter tube, d_{co} (mm)	0.5
Inside diameter of mandrel, d_{mi} (mm)	2.3
Outside diameter of mandrel, d_{mo} (mm)	2.5
Inside diameter of shield, d_{si} (mm)	4.5
Outside diameter of shield, d_{so} (mm)	4.8
Length of heat exchanger, L (mm)	50
Straight length of tube (mm)	549.5
Diameter of helical coil, D_{hel} (mm)	3.5
Pitch of tube (mm)	1.0
Number of turn of tube	50
Height of fin (mm)	0.25
Pitch of fin (mm)	0.3
Thickness of fin, t (mm)	0.1
Fin density (fins/mm)	3.3

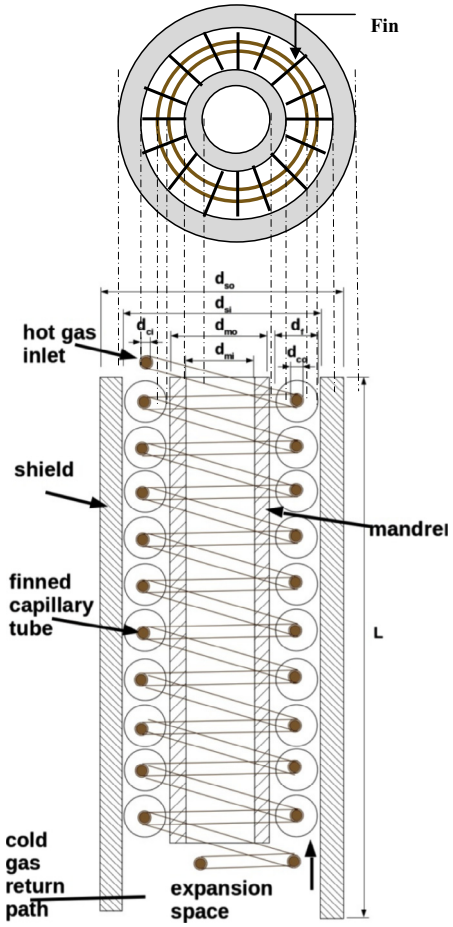

Fig. 2. Cross-sectional view of J–T heat exchanger.

$$p_{co} = \pi^2\left[\frac{n}{2}(d_f^2 - d_{co}^2) + d_{co}(1 - nt)\right]\frac{D_{hel}}{d_f} \tag{5}$$

Hydraulic diameter for return stream for pressure drop estimation is calculated as

$$D_h = \frac{4A_c}{\text{Wetted perimeter}}$$

2.1.3. Assumptions

The assumptions made in the numerical modeling of the heat exchanger for J–T cryocooler are as given below.

1. Heat transfer is one dimensional along the axis of heat exchanger.
2. Heat conduction in radial direction across the capillary wall is neglected.
3. The helical tube is assumed to be perfectly circular and closely spaced.
4. Diametrical clearance between fins and shield is neglected.
5. The emissivity of the shield is assumed to be constant with respect to variation in shield temperature.

2.2. Governing equations and boundary conditions

2.2.1. Governing equations

The governing equations used in the numerical model are as follows:

Continuity equation:

$$\frac{d\dot{m}}{dx} = \frac{d(GA)}{dx} = 0 \tag{6}$$

where $\dot{m} = \rho u A = GA$.

Momentum equation:

$$\frac{dP}{dx} = -\frac{2fG^2}{\rho d} - G^2\frac{d(1/\rho)}{dx} \tag{7}$$

where the fanning friction factor for flow in a helical coil, f is given by

$$f = 0.184\left(1 + 3.5\frac{d_{ci}}{D_{hel}}\right) \times \mathrm{Re}^{-0.2}$$

Energy equations:

$$\text{(a) Hot fluid}: \quad \dot{m}_h Cp_h \frac{dT_h}{dx} = h_h p_{ci}(T_w - T_h) \tag{8}$$

$$\text{(b) Cold fluid}: \quad \dot{m}_c Cp_c \frac{dT_c}{dx} = h_c[p_{co}(T_c - T_w) + p_{si}(T_c - T_s) + p_{mo}(T_c - T_m)] \tag{9}$$

$$\text{(c) Finned capillary tube}: \quad k_w A_w \frac{d^2T_w}{dx^2} = h_h p_{ci}(T_w - T_h) + h_c p_{co}(T_w - T_c) \tag{10}$$

$$\text{(d) Mandrel}: \quad k_m A_m \frac{d^2T_m}{dx^2} = h_c p_{mo}(T_m - T_c) \tag{11}$$

$$\text{(e) Shield}: \quad k_s A_s \frac{d^2T_s}{dx^2} = h_c p_{si}(T_s - T_c) + h_r p_{so}(T_s^4 - T_a^4) \tag{12}$$

Convective heat transfer coefficient for hot side fluid for single phase turbulent flow, $Re > 1 \times 10^4$ is given in Eq. (13).

$$h_h = 0.023 \times Cp_h G_h \mathrm{Re}_h^{-0.2}\mathrm{Pr}_h^{-2/3}\left(1 + 3.5\frac{d_{ci}}{D_{hel}}\right) \tag{13}$$

Convective heat transfer coefficient for cold side fluid for turbulent flow, $2.0 \times 10^3 < Re < 3.2 \times 10^4$ is given in Eq. (14).

$$h_c = 0.26 \times Cp_c G_c \mathrm{Re}_c^{-0.4}\mathrm{Pr}_c^{-2/3} \tag{14}$$

2.2.2. Boundary conditions

Adiabatic boundary conditions are used at both, the hot and the cold ends of the heat exchanger which are given in Eqs. (15) and (16), respectively.

$$\text{At } x = 0,\ T_h = T_{h,in},\ \frac{dT_w}{dx} = 0,\ \frac{dT_s}{dx} = 0,\ \frac{dT_m}{dx} = 0,\ P = P_{h,in} \tag{15}$$

$$\text{At } x = L,\ T_c = T_{c,in},\ \frac{dT_w}{dx} = 0,\ \frac{dT_s}{dx} = 0,\ \frac{dT_m}{dx} = 0,\ P = P_{c,in} \tag{16}$$

The above governing Eqs. (6)–(12) are solved over the control volume using finite difference technique in MATLAB. It is an accurate method as compared to segmental approach since the conduction and radiation losses can be considered in this method. The numerical solution to the descretized form of the governing equations is obtained using Gauss–Seidel iterative method. The Gauss–Seidel method requires much less memory than the direct matrix solution method and requires less computational effort as well. At each node, temperatures are initialized using a set of reasonable guess values. The finite difference equation that results from an energy balance on each control volume is solved explicitly for the temperature of the node, $T(i)$, as a function of the temperatures of the surrounding nodes. Properties are updated with local temperature and pressure conditions in the simulation. All properties of the working fluid are evaluated using BWR-S equation of state in aspenONE software [9].

3. Validation of the model

The numerical model developed is validated against the experimental results available in the literature [1]. Figures 3 and 4 show the comparison of predicted temperature profiles for two different cases of supply pressures of 179 and 140 bar, respectively, when the working fluid is argon. It is clear from these figures that the temperature profiles for the hot fluid are in good agreement with the experimental results. However, the temperature profiles of the cold fluid do not match very well. It over predicts the temperatures which indicates that the theoretically computed rate of heat gain by the cold fluid is higher. It means that, in actual case there is inefficient heat transfer between the cold fluid and the outside surface area of the finned tube. This may be due to reduction in actual heat transfer area because of non-uniform flow distribution over the finned surface. In other words, effective heat transferring area which interacts with the cold fluid on the shell side is less. Therefore, it necessitates the use of area correction factor to compute effective heat exchange area for the return stream. This is also pointed out by Chua et al. [4] without giving actual value for the same.

In the present work, the area correction factor is determined for the heat transfer area on the cold side. The relevant condition for area correction factor is to validate the numerical results against the experimental data reported by Ng et al. [1] for different operating conditions. This is probably the only experimental data available in the literature for temperature profiles in a miniature J–T cryocooler. The wetted outside perimeter of the heat exchanger is reduced step-by-step to study its effect on the temperature profiles. The numerical analysis is performed systematically in order to achieve the minimum difference between the predicted and the experimental temperature profiles for different operating conditions. It is noted that, with the decrease in surface area on the cold side, temperatures of the cold fluid decrease, while there is not much change in the temperatures of the hot fluid. Using area correction factor of 0.3, the predicted and the experimentally obtained temperature profiles show a reasonably close match. It means that the effective heat transfer area is 70% of the actual area on the cold side. A further reduction in the theoretical area shows mismatch in the predicted and the experimentally obtained temperature profiles of the hot and the cold fluid.

Figures 5 and 6 show the temperature profiles for area correction factor equal to 0.3. These figures reveal that the temperature profiles obtained with the correction factor are in good agreement with the experimental data for both the cases of the supply pressures. These figures also compare the pressure distribution of the hot fluid with that reported by Ng et al. [1] for both the cases of the supply pressure. The total pressure drop in the hot fluid is 108.7 bar for the case of supply pressure of 179.12 bar, whereas it is 71.7 bar when the supply pressure is 140.47 bar. The hot fluid pressure profiles are in close approximation with the results given in the literature [1].

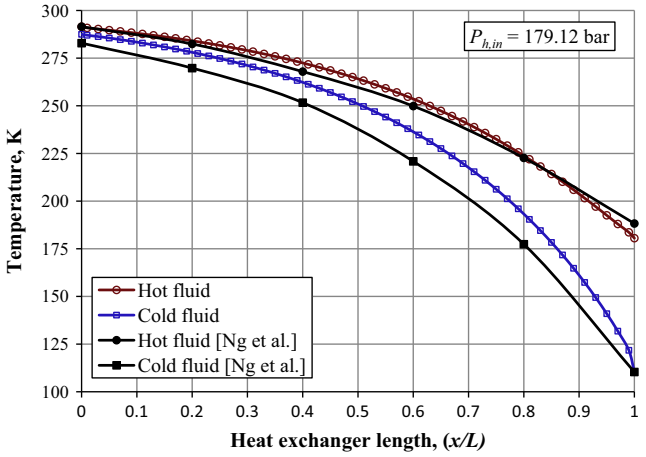

Fig. 3. Temperature profiles ($P_{h,in}$ = 179.12 bar).

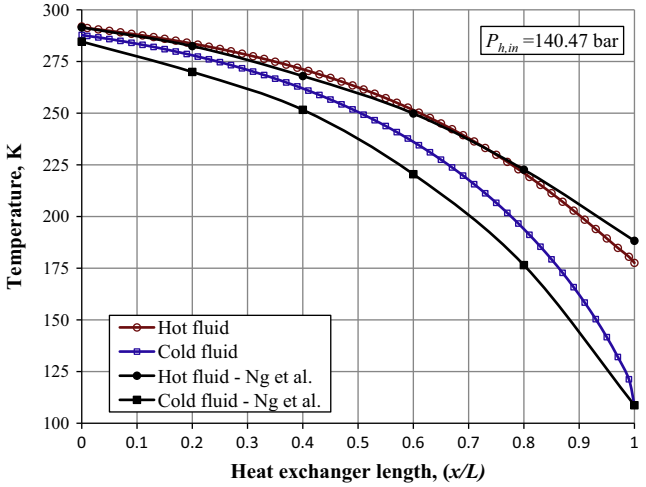

Fig. 4. Temperature profiles ($P_{h,in}$ = 140.47 bar).

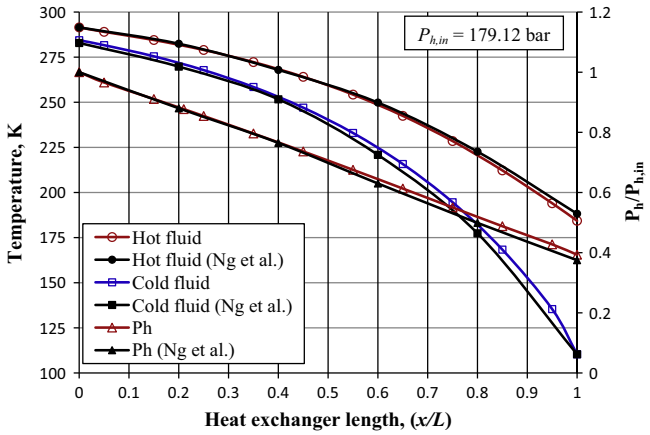

Fig. 5. Temperature profiles with area correction factor ($P_{h,in}$ = 179.12 bar).

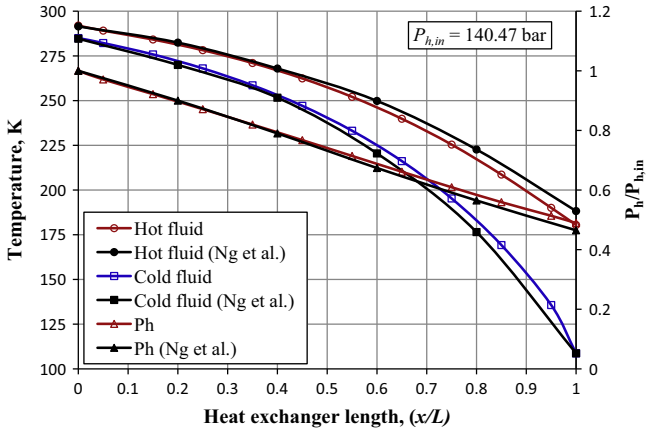

Fig. 6. Temperature profiles with area correction factor ($P_{h,in}$ = 140.47 bar).

The predicted temperatures of the cold fluid at the outlet of the heat exchanger are compared with the experimental data and the simulation results from the literature. Table 2 gives the validation of the numerical results in tabular form for the outlet temperature of the cold fluid as well as relative errors between predicted and actual results. Table 3 compares the results for pressure drop in both, the hot and the cold fluid against the literature data. It is noted that the pressure drop in both, the hot and the cold fluid, are comparable with that of the literature values. It is clear from Table 2 that the predicted temperature of the cold fluid at the outlet is close to experimental values. The relative error in the simulated results for the outlet temperatures of the fluid are within 1% limit.

4. Performance optimization of cryocooler

Performance of the J–T cryocooler depends on various design and operating parameters. The design parameters considered in the present work are fin density, coil diameter, heat exchanger length, while the operating parameters considered are working fluid, mass flow rate, and supply pressure. In the following section, effect of design parameters is studied for a J–T cryocooler, specifications of which are given in Table 1, while in the later section, the performance optimization is attempted for this specific design of the J–T cryocooler. The optimization is carried out to maximize cooling capacity at low temperature for which J–T cryocooler is designed. The parameters optimized are heat exchanger length, pressure, mass flow rate for different working fluids, argon and nitrogen. The constraints in optimizing different parameters are as given below.

(a) The condition of the hot stream at the outlet of the heat exchanger should be such that the state of the working fluid after isenthalpic expansion should fall in vapor dome so as to have sufficient cooling effect.
(b) Pressure drop in the return line should be kept minimum so that the net pressure at the return line outlet remains above atmospheric pressure.

4.1. Effect of geometry on performance of the cryocooler

The effect of the design parameters of the heat exchanger such as fin density, helical coil diameter on the performance of the cryocooler is studied to determine its optimum performance.

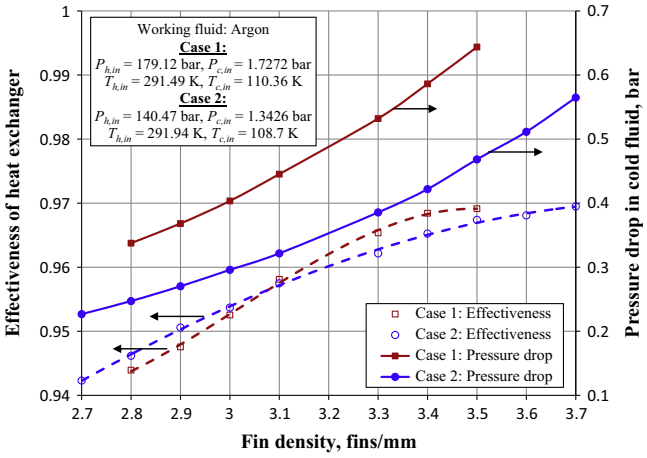

Fig. 7. Effect of fin density on the heat exchanger performance.

4.1.1. Effect of fin density on heat exchanger performance

Fin density is optimized with the objective of maximizing effectiveness of the heat exchanger and with the constraints of allowable pressure drop in the cold fluid. Fig. 7 shows the effect of fin density on the effectiveness of the heat exchanger for the case with the supply pressure of 179.12 bar and 140.47 bar. It is observed that with the increase in fin density, the effectiveness of the heat exchanger increases due to increased area of heat transfer. However, increase in effectiveness is less beyond certain fin density, i.e. 3.3 fins per mm. This is due to more resistance to flow on the cold side. Fig. 7 also shows the effect of fin density on the pressure drop in the cold fluid for both the cases of supply pressures. It is noted that the pressure drop on cold side increases with increase in fin density for both the cases of supply pressures. It is also found that the pressure drop in the cold fluid increases with the increase in supply pressure for any value of fin density. The pressure drop in the cold fluid is more crucial since increased pressure drop leads to more power consumption. The allowable pressure drop in the cold fluid for the case of supply pressure of 179 bar is 0.7 bar, while it is 0.35 bar for the case of supply pressure of 140 bar. Therefore, optimum fin density for both the operating pressures is 3.3.

4.1.2. Effect of helical diameter of heat exchanger on performance of the cryocooler

In order to study the effect of the helical diameter of the heat exchanger on the performance of the cryocooler, two cases of the helical diameters, 3.5 mm and 4.5 mm are considered. The heat

Table 2
Prediction of heat exchanger temperatures.

Input conditions				$T_{c,out}$ (K) (Ng et al. [1])		$T_{c,out}$ (K) numerical	Relative error (%)
$P_{h,in}$ (bar)	$P_{c,in}$ (bar)	$T_{h,in}$ (K)	$T_{c,in}$ (K)	Experimental	Numerical		
179.12	1.7272	291.49	110.36	282.57	282.85	284.38	+0.63
169.86	1.7460	291.40	110.42	283.73	282.90	285.53	+0.63
160.1	1.6362	292.25	109.9	284.77	284.07	285.23	0.161
149.66	1.4713	292.14	109.28	284.90	284.19	284.74	−0.056
140.47	1.3426	291.94	108.70	284.98	284.15	284.96	−0.007

Table 3
Prediction of pressure drop.

$P_{h,in}$ (bar)	$P_{c,in}$ (bar)	Pressure drop (bar) (Ng et al. [1])		Pressure drop (bar)	
		Hot fluid	Cold fluid	Hot fluid	Cold fluid
179.12	1.7272	109.26	0.67	108.69	0.529
140.47	1.3426	77.25	0.3176	71.7	0.385

transfer area is kept constant for both the cases. Therefore, the length of the heat exchanger decreases to 38.9 mm from 50 mm with the increase in helical diameter from 3.5 mm to 4.5 mm. The cooling capacity is calculated at 110 K keeping all the parameters constant for both the cases. Supply pressure for argon is fixed at 200 bar.

Fig. 8 gives the comparison of the cooling capacity variation with respect to mass flow rate for two different cases of the helical diameter. It is observed that the cooling capacity is more for the heat exchanger having less helical diameter. This is due to higher turbulence due to secondary flows in the heat exchanger. Due to increase in the helical diameter, the heat transfer rate decreases while there is compensation in pressure drop in the cold fluid due to reduced flow path for the cold fluid. Therefore, the decrease in the maximum cooling capacity is only 3.7% with the increase in the helical diameter for the above case. The maximum cooling capacity corresponds to the same mass flow rate of 0.28 g/s for both the cases.

4.2. Effect of operating parameters on performance of the cryocooler

In this section, the effect of the working fluid and other operating parameters such as mass flow rate, supply pressure on the cooling capacity is analyzed to determine the optimum performance of the cryocooler.

4.2.1. Effect of working fluid

Usually, nitrogen and argon are used as working fluids in the J–T cryocooler. The properties of the fluid significantly affect the performance of the cryocooler. In a perfect recuperator (i.e. one with an infinite conductance), maximum possible refrigeration capacity per unit mass flow is the minimum value of the specific enthalpy difference (isothermal J–T effect) over the entire operating temp range. In order to study the effect of fluid on the performance of the cryocooler, ideal cooling capacities are calculated for two different fluids: nitrogen and argon. Figures 9 and 10 show variation in the specific enthalpy difference with respect to supply pressure for argon and nitrogen, respectively. It is observed that the enthalpy difference between the two pressures decreases at higher temperatures since gas behaves more like an ideal gas. The minimum enthalpy difference at temperature of 300 K increases with the increase in supply pressure up to 40 MPa. At pressures higher than 40 MPa, the increase in ideal cooling capacity is less for argon; however, there is decrease in cooling capacity in the case of nitrogen for increase in supply pressure beyond 40 MPa. The maximum

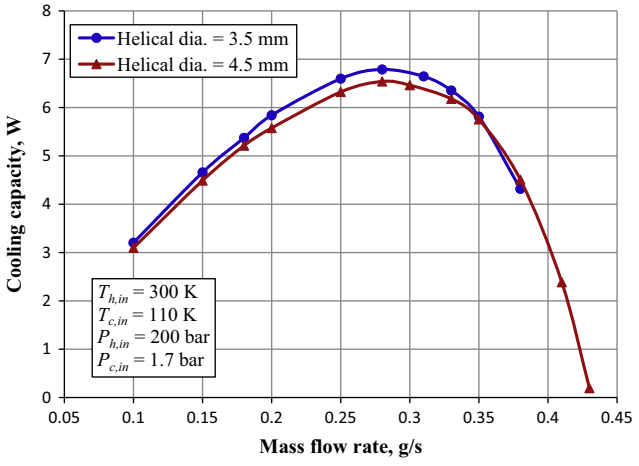

Fig. 8. Effect of helical diameter on performance of the cooler.

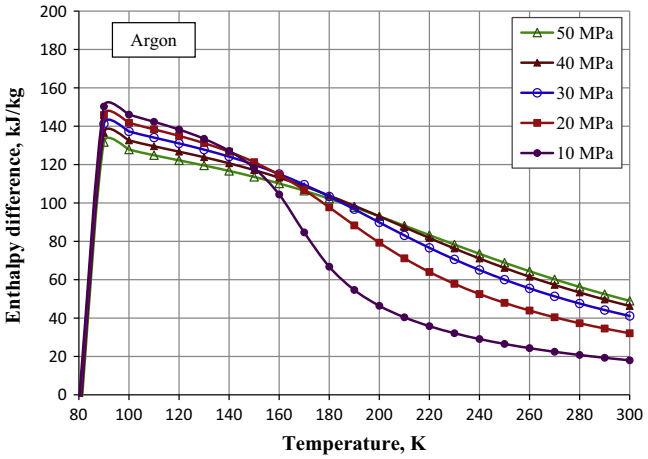

Fig. 9. Ideal cooling capacity for argon.

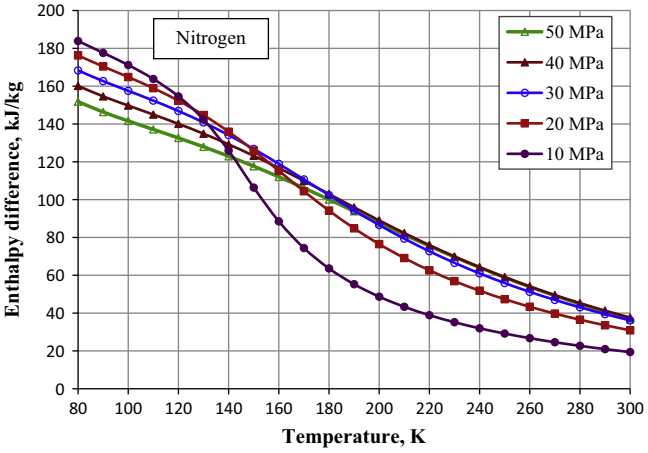

Fig. 10. Ideal cooling capacity for nitrogen.

possible cooling capacity of the J–T cryocooler with the use of nitrogen and argon is compared in Table 4. It is noted that the ideal cooling capacity for argon is more than that for nitrogen for the same operating range of temperatures and pressures.

Fig. 11 compares the cooling capacity of the J–T cryocooler working with argon and nitrogen for the same operating conditions. As pointed out in Table 4, it is found that the cooling capacity for argon at 110 K is more than that for nitrogen at any operating mass flow rate of the fluid. The difference in the cooling capacity increases with the increase in the mass flow rate. The maximum cooling capacity obtained is 6.79 W at the mass flow rate of 0.28 g/s for argon. In the case of nitrogen, the maximum cooling capacity is 4.0 W only at the mass flow rate of 0.22 g/s. This is due to reduced isothermal J–T effect for nitrogen as a working fluid. Fig. 11 also proves that the pressure drop in the hot fluid is more in the case of nitrogen as compared to that for the argon. Due to cumulative effect of increased pressure drop in the hot fluid and reduced isothermal J–T effect, cooling capacity is lower with the nitrogen as a working fluid.

The pressure drop in the hot fluid is 46.8 bar corresponding to maximum cooling capacity at 0.28 g/s for the case of argon. For nitrogen, this pressure drop is 43.3 bar corresponding to maximum cooling capacity at 0.22 g/s. It is also noted from Fig. 11 that pressure drop in the hot fluid increases significantly with increase in the mass flow rate. In the case of argon, the pressure drop in the hot fluid increases to 89.9 bar for mass flow rate of 0.38 g/s.

Table 4
Maximum cooling capacity per unit mass flow rate at various supply pressures ($P_{h,\ in}$) and $P_{c,in}$ = 1 bar.

Fluid	Temp. range	Specific enthalpy difference (kJ/kg) at supply pressure in MPa				
		10	20	30	40	50
N_2	80–300 K	19.40	30.90	36.16	37.62	36.73
Ar	90–300 K	18.0	32.10	41.10	46.30	48.99

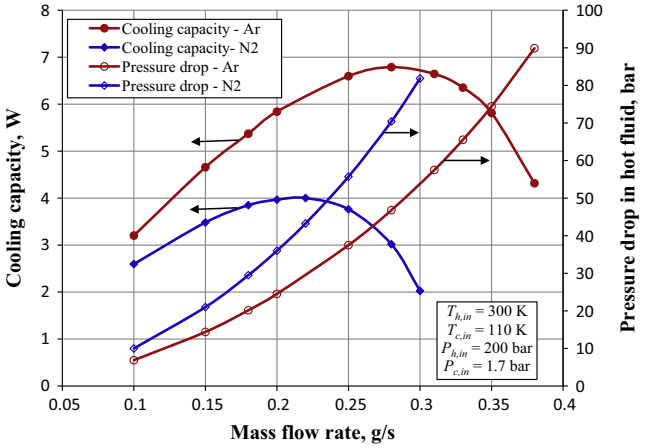

Fig. 11. Effect of working fluid on performance of J–T cryocooler.

4.2.2. Effect of mass flow rate on performance of heat exchanger

Fig. 12 shows the effect of mass flow rate on the effectiveness of the heat exchanger and pressure drop in the hot fluid. It is found that, pressure drop in the hot fluid increases significantly and effectiveness of the heat exchanger decreases with the increase in mass flow rate.

4.2.3. Effect of supply pressure on performance of the cryocooler

Fig. 13 shows the effect of supply pressure of argon on the performance of the cryocooler for the input conditions of $T_{h,in}$ = 300 K, $T_{c,in}$ = 110 K, and $P_{c,in}$ = 1.7 bar. It is clear from the figure that cooling capacity increases with the increase in supply pressure. It can also be seen that the optimum mass flow rate for producing maximum cooling capacity increases with the increase in supply pressure. The optimal mass flow rate is 0.18 g/s for the supply pressure of 150 bar, while it increases to 0.28 g/s for the supply pressure of 200 bar. Also, pressure drop in the hot fluid decreases with increase in supply pressure. The pressure drop in the hot fluid is

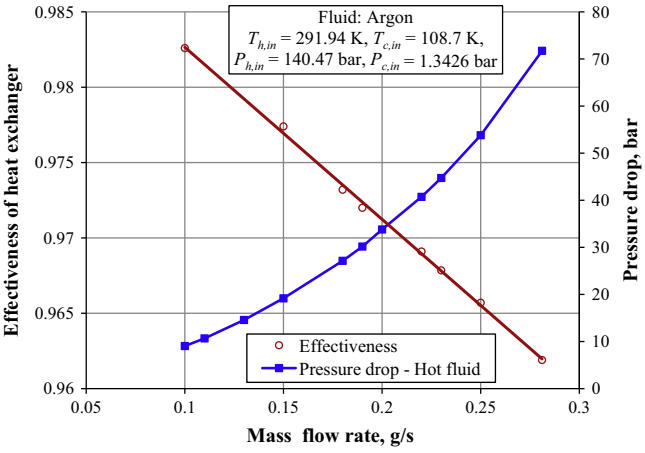

Fig. 12. Effect of mass flow rate on performance the heat exchanger.

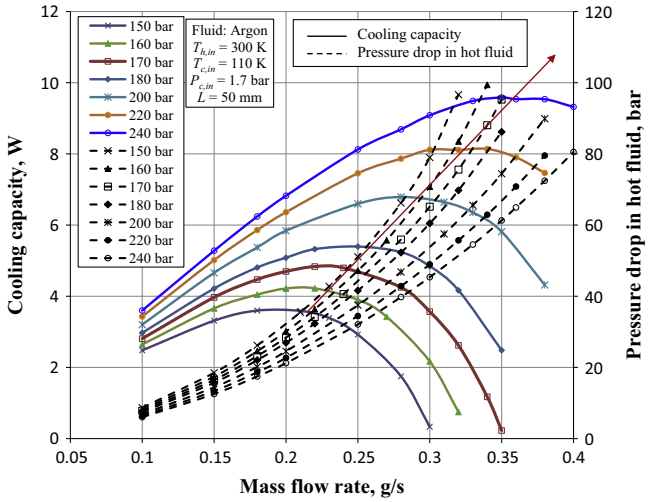

Fig. 13. Effect of supply pressure on performance of the cryocooler.

calculated to be 46.8 bar for the supply pressure of 200 bar, while it is 39.8 bar for the supply pressure of 240 bar with mass flow 0.3 g/s. This is due to the fact that both, the friction factor and the density increase with the increase in the supply pressure. However, increment in the density is more than increment in the friction factor. Therefore, the cooling capacity is more with increase in supply pressure for any operating condition of mass flow rate. Additionally, it is observed that the increase in mass flow rate beyond 0.35 g/s leads to increased pressure drop in the cold fluid. For the supply pressure greater than 180 bar, the pressure drop in the cold fluid is more than the allowable limit to have positive pressure at the suction to the compressor. Therefore, maximum limit on the operating mass flow rate is 0.35 g/s for the supply pressures greater than 180 bar. However, for the lower supply pressures, limit on the maximum mass flow rate is determined due to cooling capacity.

On the basis of above study, the optimum size of the heat exchanger to have maximum cooling capacity at low temperature of 110 K is determined for the given operating conditions. For this, high pressure and low pressure are 200 bar and 1.7 bar, respectively. It is clear from Fig. 13 that, for the heat exchanger length of 50 mm, a maximum cooling capacity of 6.8 W at 110 K can be achieved with supply pressure of 200 bar and mass flow rate of 0.28 g/s. Also, for lower mass flow rate of 0.2 g/s, the cooling capacity obtained is 5.84 W; however, this is not the maximum cooling capacity that can be obtained from the specified heat exchanger. Therefore, an optimum size of the heat exchanger should be found out for the specific mass flow rate.

Fig. 14 shows the variation in cooling capacity with respect to the heat exchanger length. Cooling capacity decreases with the increase in length beyond optimum value because of increase in pressure drop in the heat exchanger. It is found from Fig. 14 that the optimum heat exchanger length required is 45 mm only, to have maximum cooling capacity of 6.84 W when the mass flow rate is 0.28 g/s. On the other hand, when the mass flow rate is

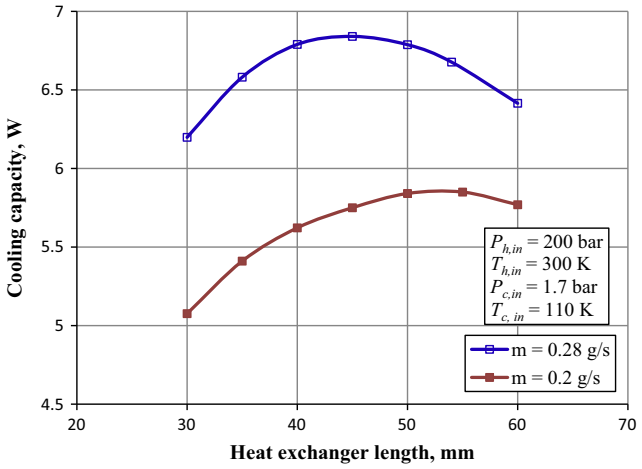

Fig. 14. Effect of heat exchanger length on performance of the cryocooler.

0.2 g/s, optimum length required is 55 mm for the maximum cooling capacity. Therefore, it can be concluded that the optimum size of the heat exchanger required is less for the higher mass flow rate conditions, when the other operating conditions are kept constant.

5. Conclusions

In the present work, a miniature J–T cryocooler is simulated using control volume approach. It is revealed that realistic heat exchange area needs to be considered for performance prediction. Based on the experimental results and model predictions, it is clear that the actual area of heat transfer is less than theoretically available heat transfer area. In view of this, a new parameter called heat transfer area correction factor is used, which confirms with the observations given by the other researchers. The numerical model followed in the present study is simple and gives realistic results with the inclusion of area correction factor.

The cryocooler performance is analyzed to determine optimum design and operating parameters. Effect of various parameters such as supply pressure, fin density, mass flow rate on the performance of the cryocooler is studied. The cooling capacity increases with increase in the supply pressure of the working fluid. The optimum mass flow rate of the fluid to have maximum cooling capacity for a given J–T cryocooler increases with the increase in supply pressure. The optimum length of the heat exchanger for given pressure and temperature conditions of the fluid decreases with increased in mass flow rate. The present work finds significance in optimization and performance comparison of the given miniature J–T cryocoolers.

References

[1] Ng KC, Xue H, Wang JB. Experimental and numerical study on a miniature Joule–Thomson cooler for steady-state characteristics. Int J Heat Mass Transfer 2002;45:609–18.
[2] Xue H, Ng KC, Wang JB. Performance evaluation of the recuperative heat exchanger in a miniature Joule–Thomson cooler. Appl Therm Eng 2001;21:1829–44.
[3] Hong Y, Park SJ, Choi YD. A numerical study of the performance of a heat exchanger for a miniature Joule–Thomson refrigerator. Cryocoolers 2009;15:379–86.
[4] Chua HT, Wang X, Teo HY. A Numerical study of the Hampson-type miniature Joule–Thomson cryocooler. Int J Heat Mass Transfer 2006;49:582–93.
[5] Chou FC, Chien SB. Preliminary experimental and numerical study of transient characteristics for a Joule–Thomson cryocooler. Cryogenics 1995;35:311–6.
[6] Chien SB, Chen LT, Chou FC. A study on the transient characteristics of a self-regulating Joule–Thomson cryocooler. Cryogenics 1996;36:979–84.
[7] Hong Yong-Ju, Park Seong-Je, Kim Hyo-Bong, Choi Young-Don. The cool-down characteristics of a miniature Joule–Thomson refrigerator. Cryogenics 2006;46:391–5.
[8] Gupta PK, Kush PK, Tiwari A. Design and optimization of coil finned-tube heat exchangers for cryogenic applications. Cryogenics 2007;47:322–32.
[9] aspenONE V 7.1. Aspen Technology Inc, Burlington, MA 01803, USA; 2009.